Malaysian Journal of Chemistry, 2023, Vol. 25(3), 184-191
(Special Issue: *2nd Applied Science Research International Conference 2022*)

The Bulk Properties and Equivalent Circuit of $CaTa_{4-x}Nb_xO_{11}$ ($0 \leq x \leq 2$)

Fadhlina Che Ros*
Physics Department, Universiti Pertahanan Nasional Malaysia, Kem Sg. Besi,
57000 Kuala Lumpur, Malaysia
*Corresponding author (e-mail: fadhlina@upnm.edu.my)

$CaTa_4O_{11}$ and solid solutions with general formula $CaTa_{4-x}Nb_xO_{11}$ ($0 \leq x \leq 2$) have been prepared and characterised using conventional solid state technique. The structures are determined on the basis of X-ray diffraction investigation which are fully indexed on hexagonal, space group $P6_322$. They consist of single layers of TaO_7 pentagonal bipyramids alternating with layers of CaO_8 octahedra. The electrical properties of these phases have been determined and all have shown excellent insulating behavior. The permittivities, ε' are in the range between 33 – 44 at room temperature which increased with the increasing Nb-dopant concentration, whilst their conductivities, σ' are too small to be measured at low temperature. The equivalent circuits have been carried out for all temperatures to identify the parameters that contribute to the data. At the lowest temperature, the equivalent circuit consists of a simple capacitor, whilst at the highest, the experimental data are modelled using a non-Debye response in series with a parallel combination of resistance and capacitance of the grain boundary.

Keywords: Bulk permittivities; $CaTa_4O_{11}$; equivalent circuit; non-Debye response; solid state

Received: August 2022; Accepted: December 2022

Calcium tetratantalum hendacaoxide ($CaTa_4O_{11}$) and lanthanum zirconium tritantalum hendacaoxide ($LaZrTa_3O_{11}$) are among the several series of compounds with general formula $A_xM_{3n+1}O_{8n+3}$. The topology of $CaTa_4O_{11}$ structure is identical to that of $LaZrTa_3O_{11}$ [1] where the structure is described as the alternations of two types of layer i.e. one layer consists of isolated edge-sharing MO_6 octahedra and a polyhedron whilst, the other consists solely of edge-sharing MO_7 pentagonal bipyramids [2-4]. The two compounds have strong similarities that the large-cations polyhedron of Ca and La are 8-coordinated, with two oxygen outside the larger faces of octahedron [1]. Detailed structure of $CaTa_4O_{11}$ has been reviewed in [2] and its description is not included. Single crystal structure of $CaTa_4O_{11}$ compound at room temperature was reported previously that it has crystalized in hexagonal, space group $P6_322$, a = 6.213, c = 12.265 Å (4, 5) which agrees to our recent findings of $CaTa_4O_{11}$ powders as hexagonal, space group $P6_322$, a = 6.208, c = 12.257 Å (2).

Literature of $A_xM_{3n+1}O_{8n+3}$ including $CaTa_4O_{11}$ compositions were focused only on their unique structural aspect of different stacking variants close in composition however, there has been less interest in the electrical properties as $CaTa_4O_{11}$ is reported to be a dielectric over a wide temperature range. Our preliminary results of $CaTa_{4-x}Nb_xO_{11}$ ($0 \leq x \leq 2$) showed that these ceramics displayed capacitance plateaus from room temperature to 500 °C with the values of 3.1, 3.5 and 4.0 pF/cm, that increased along with the increasing of x which may attributable to the bulk response. These samples were also found too resistive to be measured at room temperature with $R >> 10^9$ Ωcm in which temperatures in excess of 500° C are required to obtain useful data. It is presumed that thorough investigation is necessary to understand their electrical behavior therefore, presented herein is the re-investigation of the $CaO – Ta_2O_5 – Nb_2O_5$ system with the motivation to study in detailed the bulk properties and their equivalent circuits carried out at wide temperature ranges from -263.15 °C to 800 °C. Analysis and modelling of impedance spectroscopy data provides useful information about the physical processes that occur within the samples which can be represented by capacitor, C, resistor, R and constant phase element, CPE components of the proposed equivalent circuit. As the appropriate electrical circuit model was selected, initial estimation of parameters such as resistor, R, capacitor, C and Constant Phase Element, CPE in the circuit was made. These initial values are used to simulate the impedance response and should show the same general features as the experimental data.

EXPERIMENTAL

$CaTa_4O_{11}$ and solid solutions were synthesised using $CaCO_3$, Sigma Aldrich (99.9%), Ta_2O_5 (Stanford Materials (99.9%) and Nb_2O_5, Stanford Materials (99.9%) powder mixtures. Dried reagents were weighed, mixed manually using an agate mortar and pestle with acetone for 20 – 30 min, pelleted and fired at different temperatures in ambient air. Samples were calcined

†Paper presented at the 2nd Applied Science Research International Conference 2022 (2nd ASRIC 2022)

overnight at 1000 °C to decarbonate the $CaCO_3$ as well as to initiate reaction. $CaTa_{4-x}Nb_xO_{11}$ ($0 \leq x \leq 2$) was obtained after heating the pellets at temperatures 1300° – 1500 °C for several days in ambient air with daily grinding.

The phases present were analysed using X-ray powder diffraction, XRD at room temperature using a Stoe StadiP diffractometer, Cu-Kα_1 radiation (λ = 1.54056 Å). External silicon standard, NIST 640d Si was used for line position calibration in which data were managed and compared against the reference data in the ICDD's PDF-2 database by using STOE WinXPOW software package. Data were collected at ~ 4 h per pattern and corrected for absorption. For electrical property measurements, pellets ~1.5 mm thick and ~ 10 mm diameter were prepared by uniaxial pressing. Pellet densities were ~ 84 to 90%. Electrodes were fabricated on opposite pellet faces from Pt paste, which was dried, decomposed and hardened by gradually heating to 900 °C. Samples with electrode attached were placed into a conductivity jig and electrical property data were recorded using a combination of Hewlett Packard 4192A and Solartron 1260/1286 impedance analysers over the frequency range 10^{-2} Hz to 1 MHz at temperature range 30° to 800 °C. For measurements that were below room temperature, an Oxford Cryostat was used and the data collected within the temperature range between -263.15 °C to 46.85 °C. Impedance data were corrected for overall pellet geometry and for the blank cell capacitance (jig correction).

RESULTS AND DISCUSSION

Reaction Conditions and Phase Identification

All samples were heated at different temperatures and times due to the level of Nb substitution at Ta site, as well as to establish conditions required to achieve equilibrium. $CaTa_4O_{11}$ and $CaTa_3NbO_{11}$ samples were prepared at 1500 °C whilst, $CaTa_2Nb_2O_{11}$ was at 1400° C. The $CaTa_4O_{11}$ phase was first detected using XRD at 1350 °C for x = 0 and 1, together with un-reacted Ta_2O_5 and Nb_2O_5 raw materials whilst, for x = 2, the phase was initially recognised at 1300 °C. The impurity peaks of Ta_2O_5 and Nb_2O_5 however, were gradually decreased as the temperature increased and this remained the same over the entire range of heating times. $CaTa_4O_{11}$ was found phase pure at 1500 °C for 24 h, $CaTa_3O_{11}$ at 1500 °C for 36 h and $CaTa_2Nb_2O_{11}$ at 1400 °C for 60 h.

Like most ionic materials, $CaTa_4O_{11}$ and $CaTa_3NbO_{11}$ have high melting points and becomes thermally stable at 1000 °C to 1500 °C; at temperature above 1500 °C, they could possibly melt or decompose. In this system, the increase of Nb content contributed to lower firing temperature and thermal stability of the structure. The highest reaction temperature for x = 2 is 1400 °C before it melts at 1450 °C, and as a results, longer firing times is required as it took 60 h to form a phase pure product compared to $CaTa_4O_{11}$ and $CaTa_3NbO_{11}$ which took 24 h and 36 h, respectively.

Figure 1 shows the experimental XRD patterns of single phase $CaTa_{4-x}Nb_xO_{11}$: x = 0, 1 and 2 samples. It is noticeable that the patterns correspond well with that reported ICDD data (PDF card 70, 847) for $CaTa_4O_{11}$. We have previously reported the cell parameters from all peak positions of $CaTa_{4-x}Nb_xO_{11}$ ($0 \leq x \leq 2$) using Rietveld refinement [6] which were indexed on a hexagonal unit cell, space group $P6_322$. Lattice parameters and the unit cell volume in this system obey Vegard's Law which depicted the formation of solid solution in this region. The increase in Nb level substitution for Ta, increases the unit cell size causing the whole pattern to shift to lower 2θ giving this systematic decrease in peak position throughout the entire range of x. XRD pattern for x = 2.5 exhibited non-identical pattern to that of $CaTa_4O_{11}$ as it contains mixture of $CaTa_4O_{11}$, $CaNb_2O_6$ and un-reacted Nb_2O_5 phases and therefore, consistent with those of previous reports that the limit solid solutions for CaO-Ta_2O_5 system is x = 2 [5]. The XRD profiles of x = 2.5 is given in the supplementary, S1.

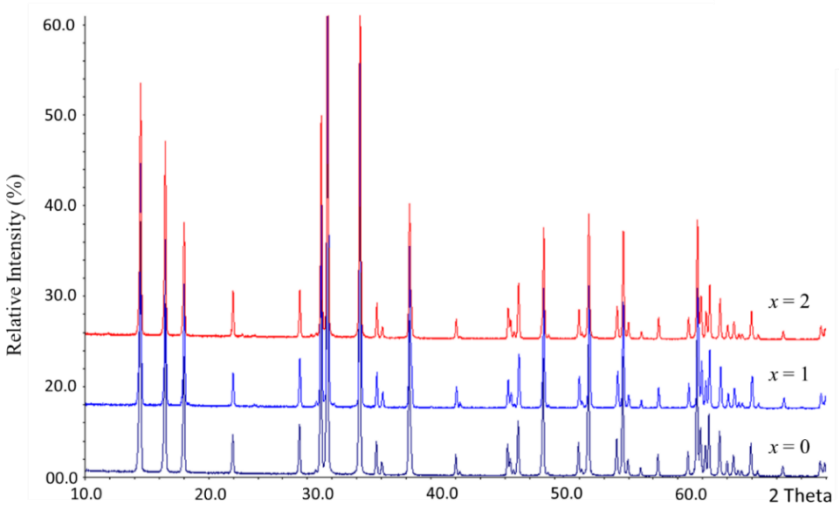

Figure 1. Diffraction patterns of $CaTa_{4-x}Nb_xO_{11}$ ($0 \leq x \leq 2$).

Table 1. Comparison of unit cell parameters between literatures and the experimental results.

Compositions (x)	Hexagonal cell dimension (Å)		Volume (Å^3)	References
	a	c		
$CaTa_4O_{11}$	6.213(1)	12.265(1)	410.01	Jahnberg, 1970
$CaTa_4O_{11}$	6.22000(5)	12.25000(5)	410.4	Gasperin, 1963
$CaTa_4O_{11}$	6.21730(3)	12.2710(2)	410.7	Isobe *et al*., 1975
$CaTa_4O_{11}$	**6.20871(7)**	**12.2573(2)**	**409.194(9)**	**Observed**
$CaTa_3NbO_{11}$	**6.21663(1)**	**12.2620(3)**	**410.53(1)**	**Observed**
$CaTa_2Nb_2O_{11}$	**6.22536(6)**	**12.2746(2)**	**411.972(8)**	**Observed**

Comparison list of $CaTa_{4-x}Nb_xO_{11}$ ($0 \leq x \leq 2$) lattice parameters with other literatures by Jahnberg, Gasperin and Isobe *et al*. as shown in Table 1 depicted insignificant difference with each other [5, 7, 9]. However, such small difference may be attributable to slight variations in stoichiometry, for example oxygen loss and/or cation non-stoichiometry arising from different processing conditions [8]. The expenditure of the unit cell is due to the Nb substitution for Ta ion, and according to Bragg's Law and *d*-spacing formula, this leads to the increase in *d*-spacing of the powder lines causing the whole pattern shifts to lower values of 2θ. Despite the fact that Nb^{5+} and Ta^{5+} have the same ionic radius (0.74 Å; coordination number, CN = 6) [10], it is assumed that the changes in the unit cell parameters are governed by the relative sizes of Nb^{5+} ions that replaced Ta^{5+} in the solid solutions mechanism [2, 10].

Bulk Properties of $CaTa_{4-x}Nb_xO_{11}$ ($0 \leq x \leq 2$) at Low Temperatures

Impedance measurement at low temperatures, -263.15 °C to 46.85 °C for all compositions have been carried out. Theoretically, the densities of the samples are 90, 84 and 86 %, respectively. Each composition shows similar dielectric behavior trend at low temperatures therefore, data at -173.15 °C was selected to represent the results of all samples. Figure 2(a) shows the comparison graph of capacitance, *C'* versus frequency, *f*, all data is depicted independent of frequency, *f* and increased with the increasing Nb content. Figure 2(b) shows the admittance, *Y'* as a function of frequency, *f* measured and the data shows temperature- and composition-independent as they overlapped with each other. It is observed that the samples were highly insulated with the value of resistance, $R >> 10^9$ Ω; indeed, *Y'* is too large that the *dc* conductivity could not be measured instead, *ac* conductivities which showed a power law response were observed.

Bulk Properties of $CaTa_{4-x}Nb_xO_{11}$ ($0 \leq x \leq 2$) at High Temperatures

The electrical properties measurement at temperature ranges between 25° to 800 °C of selected frequencies were measured. The capacitance, *C'* data from the room temperature of 400 °C for all compositions showed similar trend of frequency- and temperature-independent behavior, which resembled those with low temperature data. The capacitance plateaus are approximately 3.1, 3.5 and 4.0 pF/cm for $x = 0$, 1 and 2 respectively, increased with the increasing Nb content which indicate the response of bulk capacitance.

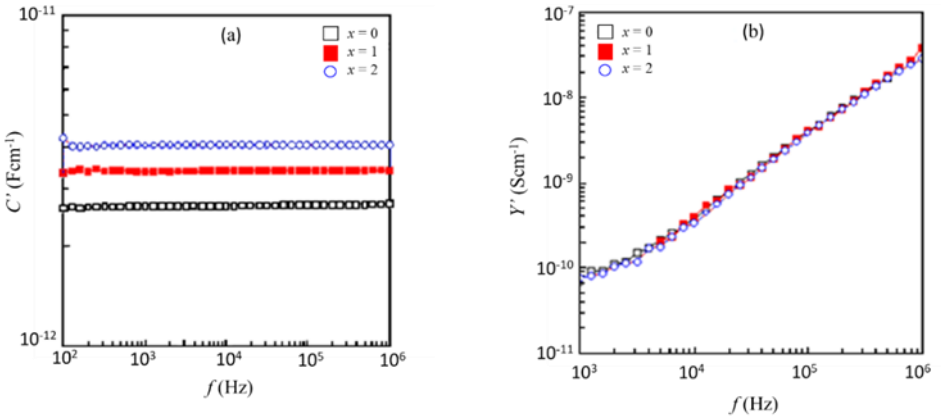

Figure 2. Impedance spectroscopy data for $x = 0$, 1 and 2 samples measured at -173.15 °C. (a) Comparison of capacitance, *C'* versus *f* data with the highest data is $x = 2$ whilst the lowest is $x = 0$, (b) The overlapped data of admittance, *Y'* versus *f*.

As the temperature increased to 500 °C and above, the capacitance data exhibit increasing values, 10^{-11} - 10^{-10} F/cm with decreasing frequency, f which might be associated with either the contribution from interfacial/ grain boundary capacitance or the non-ideality of bulk response, CPE, where the most pronounced increment shown is at x = 2 composition, Figure 3. Evidently, low frequency dispersion of capacitance, C' for all samples are shifted to higher frequencies as the temperature increased, which implies that thermally-activated resistances are involved in this frequency region (see Figures 3(a, b)). The low conductivity trend of these ceramics have been reported previously [2] in which the total conductivity was measurable only at temperature above 600 °C. The trend suggests the insulating behavior of the ceramics which is parallel with the reported high values of activation energy, $E_A \sim 0.96$ eV, 1.72 eV and 1.76 eV for x = 0, 1 and 2, respectively [2].

At the highest temperature ~ 800 °C, the complex plane plot, Z^* for x = 0 and 1 produced broad and overlapping arcs as shown in Figure 4(a), whilst for x = 2, two arcs were detected, Figure 4(b); high frequency corresponds to bulk response whilst grain boundary at lower frequency. The presence of non-ideal Debye peaks were clearly observed in the combined plot of M'' and Z'' for all samples; the full width at half maximum (FWHM) value at M' peaks are ~ 1.5 on a log scale which deviate significantly from the ideal value: 1.14 decades. Figure 4(c) shows the plot of M'' and Z'' vs. frequency for x = 2. In view of electrical heterogeneity of the materials, it is necessary to identify the correspond equivalent circuit at every temperature in order to parameterise the data.

Measurement at high frequency region, $f > 10^4$ showed the capacitance, C' data depicted frequency-independent behavior for all samples, however, the plateaus data are not exactly frequency independent even at 1 MHz. By extrapolating the capacitance, C' data at 1 MHz to infinite frequency, C_∞ an estimation value of bulk capacitance, C_b can be determined, as shown in Figure 4(c, d). The bulk capacitance, C_b values were obtained using formula $C' = \varepsilon' (A/d)$ and converted to permittivity, ε_∞, Table 2 indicates where the values increased with the increasing of Nb content. At room temperature, the measured bulk permittivity, ε_∞ at 1 MHz are inconsistent with the values at GHz since the permittivity decreased with the increasing frequency. The lesser stability of permittivity at micro-wave region, GHz may indicate that they are not suitable for microwave application [12].

Table 2. Comparison permittivities of $CaTa_{4-x}Nb_xO_{11}$ ($0 \leq x \leq 2$).

Compositions	Density (%)	Permittivity, ε' at - 263.15 – 46.85 °C	Permittivity, ε_∞ at MHz	Permittivity, ε' at GHz
$CaTa_4O_{11}$	90	33	32.5 – 35.4	22
$CaTa_3NbO_{11}$	84	40	39.2 – 39.6	25
$CaTa_2Nb_2O_{11}$	86	44	40.6 – 44.0	31

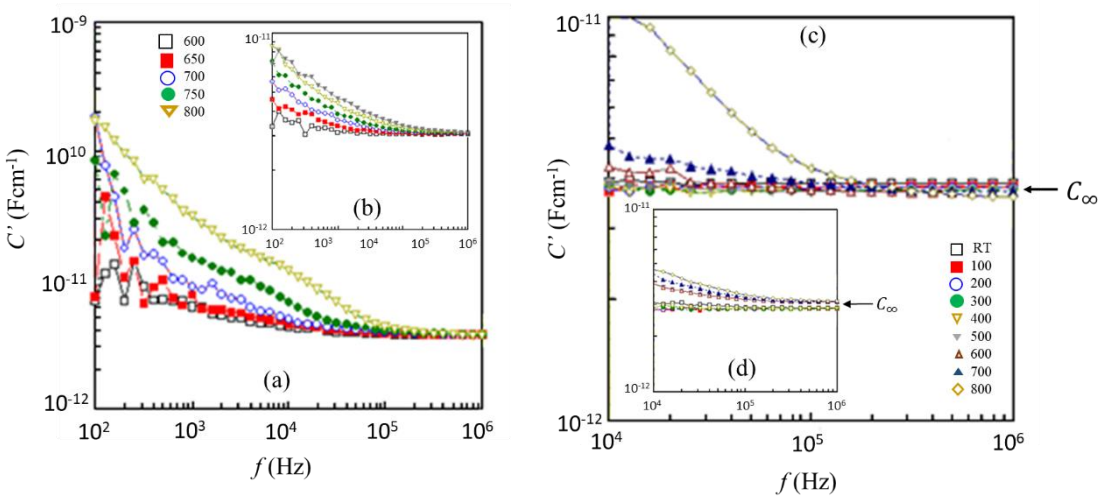

Figure 3. The capacitance, C' plot versus f at high temperatures for (a) x = 2, (b) x = 0 and the magnifying image of spectroscopic plot for C' versus f from room temperature – 800 °C at 10 kHz to 1 MHz for (c) x = 2 and (d) x = 0; the arrow signs indicated the C_∞.

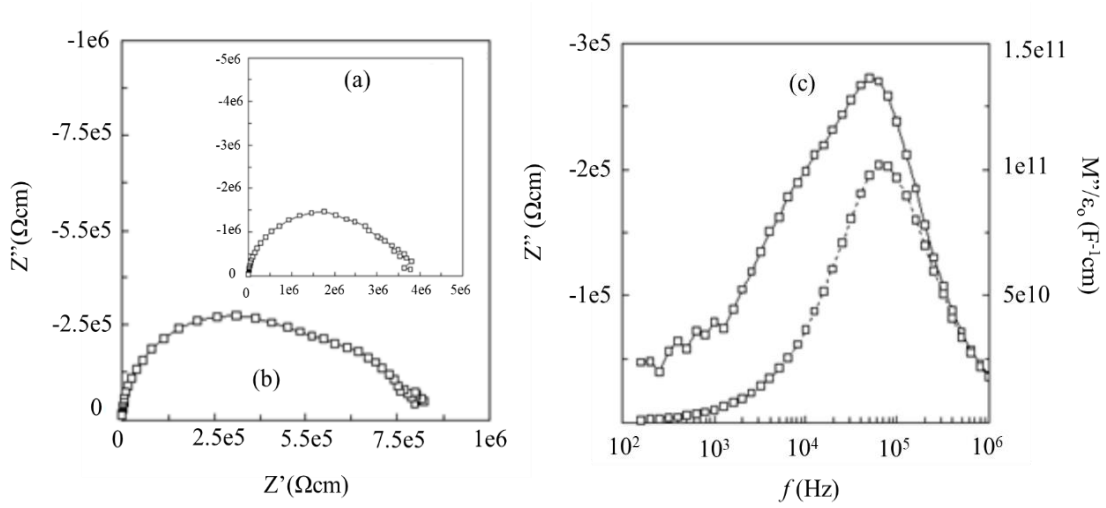

Figure 4. Cole-Cole plots of (a) $x = 1$ and (b) $x = 2$ whilst (c) is *Z", M"* versus *f* plot for $x = 2$.

Equivalent Circuit Analysis

Physical interpretation which characterises the insulating behavior of the samples can be recognised by equivalent circuit that can accurately represents the electrical properties. It is necessary to identify which parameters contribute to the impedance data of $CaTa_{4-x}Nb_xO_{11}$ ($0 \leq x \leq 2$). A fitting program, ZView Equivalent Circuit software was used to model the impedance data; selection of the frequency range is crucial so as to avoid any unreliable and/or irregular data due to the limit of instrument and resonance effect. Modelling of the data usually starts with the bulk response at low temperatures and gradually increased to higher ones where for each temperature, visual inspection data of different formalisms were performed to figure the correct circuit. Hence, an approximate values of resistor, capacitor and other element may be presumed to simulate the impedance response and should portrait similar general feature as the experimental data. The circuit element parameter can be varied at different settings for example in this study, the bulk parameters were fixed in order to enable fitting at high temperature data whilst the rest are set as free (+) to eliminate invalid negative values.

In this work, the modelling phases are divided into three sections: i) low temperature range ≤ 500 °C, ii) intermediate range 500° – 600 °C and iii) high temperature range, 650° – 700 °C and the equivalent circuits are shown in Figure 5. By visual inspection, data at low temperature ≤ 500 °C displayed features that indicated a bulk response of ceramic which is represented by a simple capacitor, C_1, as shown in Figure 5(a); this includes the data at temperature range -263.15 °C to 46.85 °C. As the temperature increased to 500° – 600 °C, the appearance of high frequency dispersion of *Y'* and low frequency dispersion of capacitance, *C'* suggested the inclusion of a CPE in parallel with C_1, as indicated in Figure 5(b). It is evident that these samples exhibited a non-ideal Debye response which is usually described by incorporating a CPE to the circuit [8].

As the temperature increased to 650° – 700 °C, measurable resistance, R_1 which is attributable to bulk resistance began to appear therefore, the electrical circuit at this temperature region can be represented by a parallel combination of R_1, C_1 and a CPE, as shown in Figure 5(c). Similar circuit satisfies impedance data at 800 °C for $x = 0$ and 1, but not for $x = 2$. For $x = 2$, the circuit can only fit at low and intermediate temperature ranges but as the temperature reached 725 °C, the impedance data were best modelled using non-Debye response circuit consisting parallel of R_1, C_1, CPE, in series with a parallel combination of resistive grain boundary, R_2 and the associated parallel capacitance, $C_2 \sim 10^{-10}$ Fcm^{-1} which is attributable to grain boundary response of the ceramic, as seen in Figure 5(d). The fitting profiles for $x = 2$ at different temperatures are shown in Figures 6 and 7. Here, we consider *C'* and *Y'* formalisms on logarithmic scales to verify the validity of the circuit. Temperature dependent trends of the fitting parameters, *C'*, *A* and *n* are shown in Figures 8 – 10.

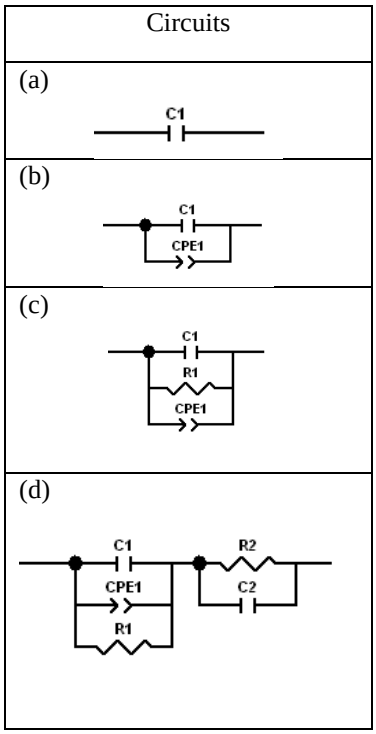

Figure 5. Equivalent circuits with different combination of *R*, *C* and CPE elements.

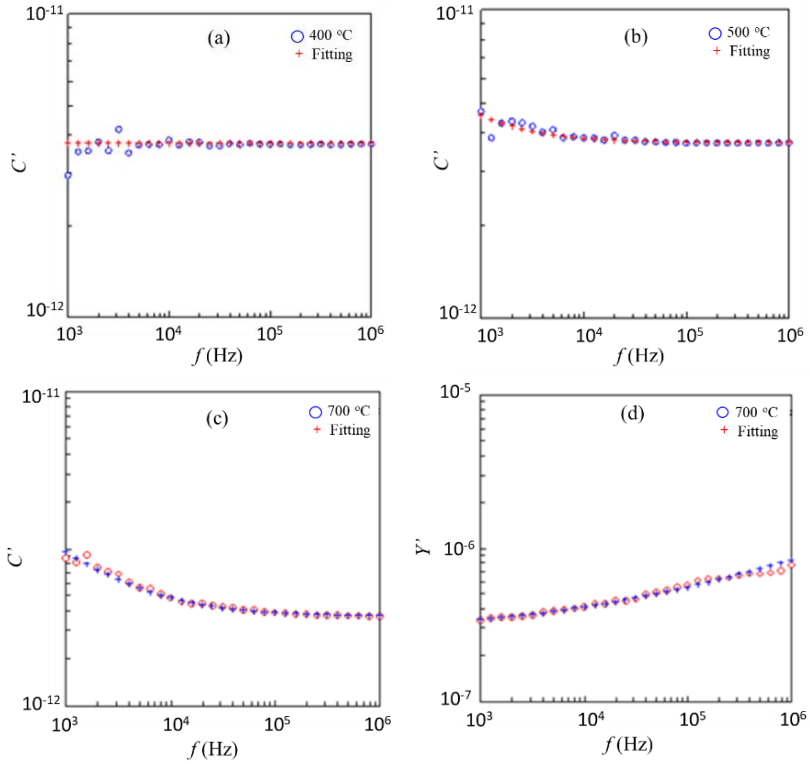

Figure 6. *C'* versus log *f* fitting data for $x = 2$ at (a) 400 °C, used circuit 5(a) and (b) 500 °C, used circuit 5(b). Figures 6(c) and 6(d) are *C'* versus log *f* and *Y'* versus log *f*, at 700 °C respectively, used circuit 5(c).

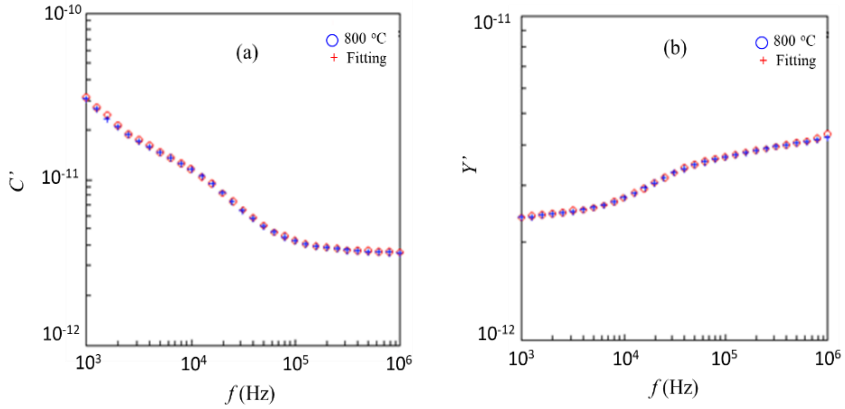

Figure 7. Experimental data of $x = 2$ at 800 °C modelled used circuit 5(d) for (a) *C'* versus log *f* and (b) *Y'* versus log *f*.

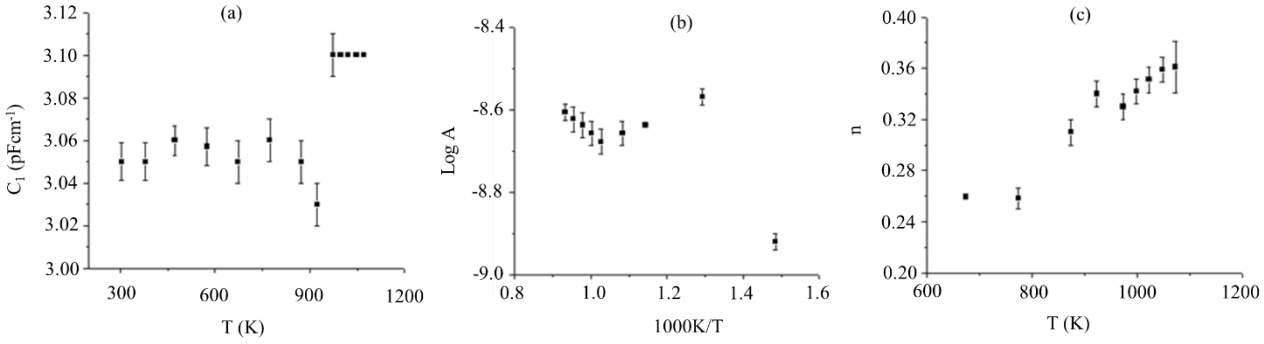

Figure 8. Temperature dependent behavior of the bulk capacitance, C_1, conductive component, A and n for $x = 0$

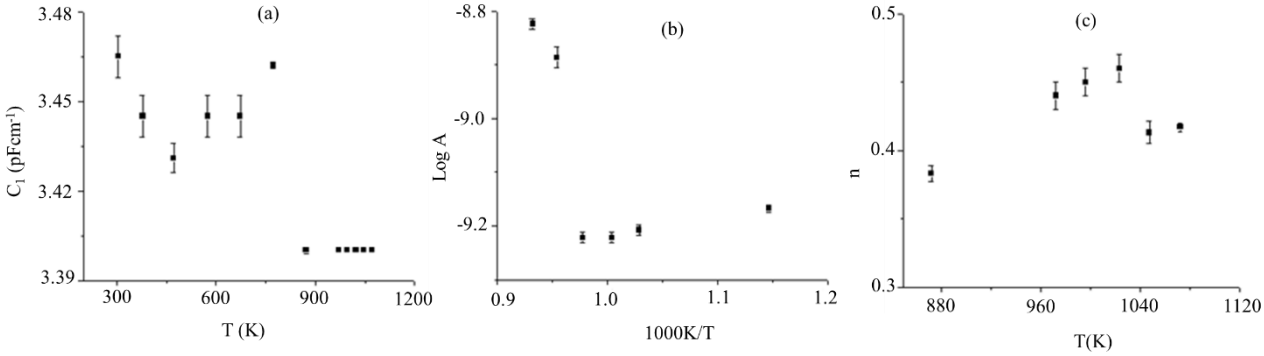

Figure 9. Temperature dependent behavior of the bulk capacitance, C_1, conductive component, A and n for $x = 1$

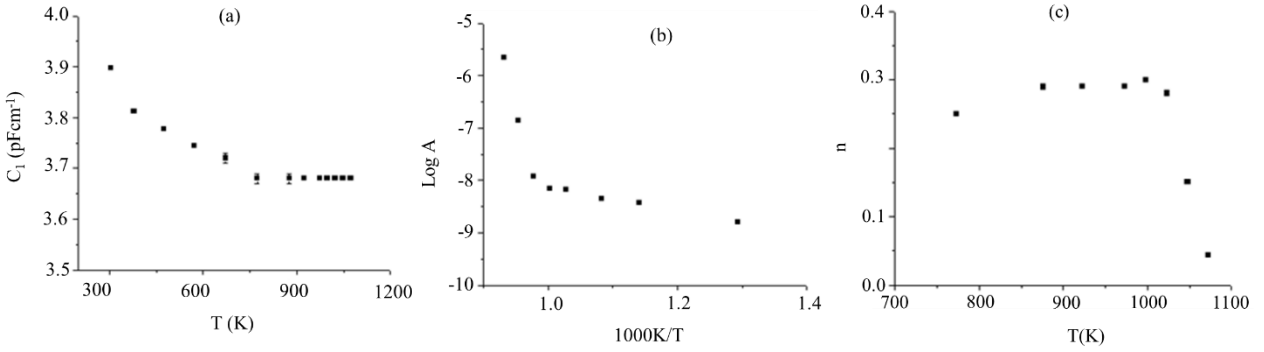

Figure 10. Temperature dependent behavior of the bulk capacitance, C_1, conductive component, A and n for $x = 2$

It is evident from Figures 3 and 4 that the samples show a non-ideal Debye response which usually described by a CPE element; CPE can be described by $Y^* = A\omega^n + jB\omega^n$ where $j = \sqrt{-1}$. The non-ideal Debye response is frequently used to model the electrical properties of ionically conducting materials and there are several occurrences that motivate the use of CPE to model the experimental data: i) the power law response in the C' data of slope (n-1) at low frequency which levels off to a frequency independent value at high frequencies, Figure 5 and ii) the value of n slope, ($0 < n < 1$) at high frequency of power law data. The circuit parameters C_1, C_2, R_1, A and n were obtained; for all samples, the magnitude of R_1 component can only be measured at temperatures above 600 °C and increases along with rising temperature. The magnitudes of the bulk capacitance, C_1 were set to a constant value starting 700 °C for $x = 0$, 1 and 500 °C for $x = 2$ or else, it will decrease with the increasing temperature, and same goes for A and n values which

represent the frequency dependent conductive component of *Y'* data and this may possibly be associated with the changing frequency range of the bulk plateau. By setting the C_1 to a certain value, this enables the high temperature data to be fitted without unreasonable data. Temperature dependent graphs, Figures 8 – 10 were extracted from the parameter values of the modelled data. It can be seen that in all compositions that the value of bulk capacitance, C_1 increased slightly, with the increasing Nb content; the value for each composition are almost constant with a slight change of temperatures. As for the conductive components, *A* and *n*, both samples show slight variant of temperature dependent.

CONCLUSION

The synthesis of $CaTa_{4-x}Nb_xO_{11}$ ($0 \leq x \leq 2$) have been carried out using conventional solid state technique. They are all single phase at different temperatures and have been indexed on a hexagonal, space group $P6_322$ which are in good agreement with the literatures. The bulk properties of $CaTa_{4-x}Nb_xO_{11}$ ($0 \leq x \leq 2$) have been characterised and overall $CaTa_{4-x}Nb_xO_{11}$ ($0 \leq x \leq 2$) have very low conductivity as temperatures in excess of 600 ^oC were required to obtain useful conductivity data. At temperatures between -263.15 ^oC and 500 ^oC, the capacitance data, *C'* are independent of frequency and temperature over the entire measurement range which indicated the response of bulk capacitance, C_b whilst above 600 ^oC the bulk conductivities are in the range 0.96 – 1.76 eV. The permittivity, ε' increased with the increasing of Nb content as much higher conductivity was observed with the increasing substitution of Ta by Nb which possibly related to the higher polarisability of Nb^{5+} compared to Ta^{5+}. The bulk permittivity at MHz and GHz frequencies were measured and showed huge differences for these materials to be of interest in microwave application. The impedance data of $CaTa_{4-x}Nb_xO_{11}$ ($0 \leq x \leq 2$) have been satisfactorily modelled by equivalent circuits. At low temperatures, the circuits are either a simple capacitor or a combination of capacitor and a CPE. As the temperature increased, the circuit is derived based on dielectric relaxation processes consisting a parallel RC element which is added to a parallel CPE.

ACKNOWLEDGEMENT

The author would like to thank Ministry of Higher Education Malaysia (MOHE) and Universiti Pertahanan Nasional Malaysia (UPNM) for providing their assistance for this research. This work is supported and funded by the Fundamental Research Grant Scheme (FRGS): FRGS/1/2017/STG07/UPNM/02/2.

REFERENCES

1. Grins, J. and Nygren, M. (1992) Structure of $LaZrTa_3O_{11}$, A $CaTa_4O_{11}$ Isotype. *Mat. Res. Bull.*, **27**, 141–145.

2. Che Ros, F. (2018) Structure, Electrical and Microwave Properties of $CaTa_4O_{11}$ and Solid Solutions Ceramics. *J. Comp. & Theo. Nanoscience*, **24**, 8908–8912.

3. Jahnberg, L. (1981) A Series of Structures Based on Stacking of α-U_3O_8-Type Layers of MO_7 Pentagonal Bipyramids, *Mat. Res. Bull.*, **16**, 513–518.

4. Ercit, T. S., Hawthorne, F. C. and Cerny, P. (1985) The Crystal Structure of Synthetic Natrotantite. *Bull. Mineral*, **108**, 541–549.

5. Jahnberg, L. (1963) Crystal Structures of $Na_2Nb_4O_{11}$ and $CaTa_4O_{11}$. *J. Solid State Chem.*, **1**, 454–462.

6. Che Ros, F. (2017) Rietveld Refinement Strategy of $CaTa_{4-x}Nb_xO_{11}$ Solid Solutions using GSAS-EXPGUI Software Package. *Mat. Sci. Forum*, **888**, 167.

7. Gasperin, M. (1963) Étude Cristallographique D'un Oxyde Double de Tantale et de Strontium. *Bull. Soc. franç Minér*., 386–388.

8. West, A. R., (1999) Basic solid state chemistry. *2nd ed. John Wiley & Sons*.

9. Isobe, M., Marumo, F., Iwai, S. and Kimura, M. (1963) Calcium Tetratantalate. *Acta Crystallogr.*, **B31**, 908–910.

10. Shannon, R. D., (1993) Dielectric properties of ions in oxides and fluorides. *J. Apply. Phys.*, **73(1)**, 348–366.

11. Almond, D. P., Duncan G. K. and West, A. R. (1983) The determination of hopping rate and carrier concentration in ionics conductors by a new analysis of ac conductivity. *Solid State Ionics*, **8,** 159–164.

12. Reaney, I. M. and Iddles, D., (2006) Microwave dielectric ceramics for resonators and filters in mobile phone networks. *J. Am. Ceram. Soc.*, **89(7)**, 2063–2072.

Supplementary Data, S1

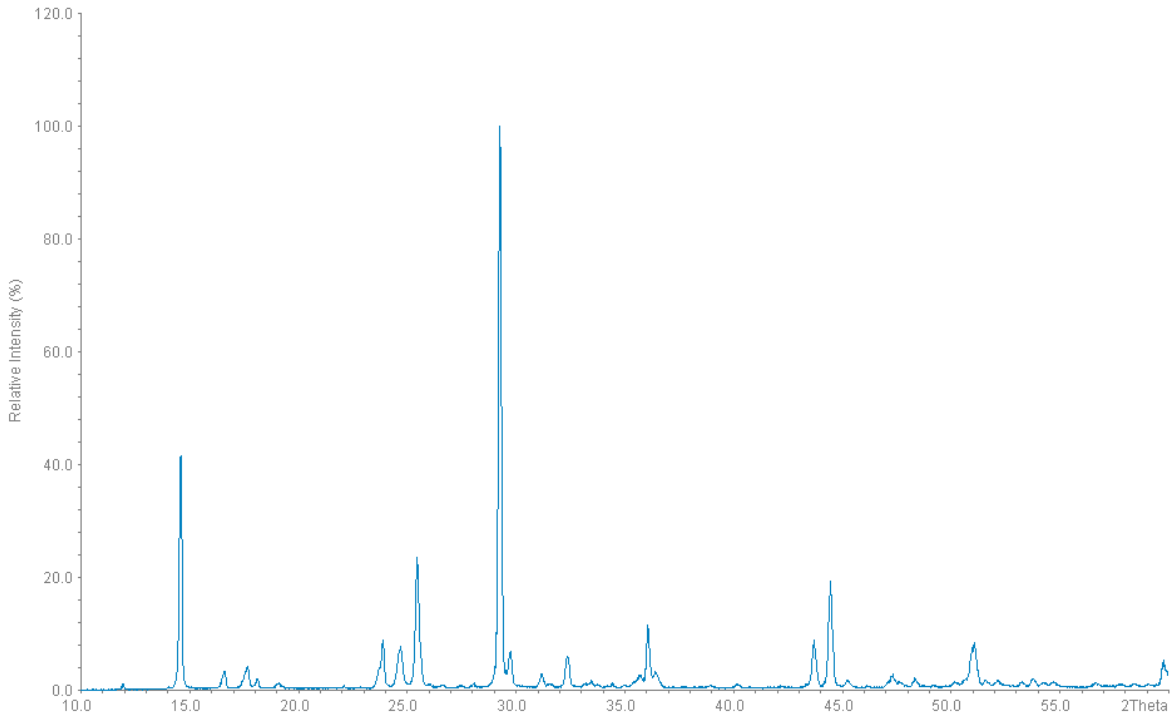

Figure 11. Diffraction pattern of $CaTa_{1.5}Nb_{2.5}O_{11}$

Supplementary Data, S2

Table 3. Fitting data for CaTa4O11 from 30 oC to 800 oC

T (ºC)	C_1 (Fcm^{-1})	A (Scm^{-1}rad^{-n})	n	R_1 (Ω cm)
30	$3.050(9) \times 10^{-12}$			
106	$3.050(9) \times 10^{-12}$			
199	$3.060(7) \times 10^{-12}$			
301	$3.057(9) \times 10^{-12}$			
400	$3.05(2) \times 10^{-12}$	$1.2(2) \times 10^{-9}$	0.26(2)	
500	$3.06(2) \times 10^{-12}$	$2.7(2) \times 10^{-9}$	0.258(8)	
600	$3.05(1) \times 10^{-12}$	$2.3(5) \times 10^{-9}$	0.31(1)	$7.1(1) \times 10^{7}$
650	$3.03(1) \times 10^{-12}$	$2.2(3) \times 10^{-9}$	0.34(1)	$3.1(2) \times 10^{7}$
700	$3.10(1) \times 10^{-12}$	$2.1(3) \times 10^{-9}$	0.33(1)	$1.30(2) \times 10^{7}$
725	3.10×10^{-12}	$2.2(3) \times 10^{-9}$	0.342(1)	$9.6(1) \times 10^{6}$
749	3.10×10^{-12}	$2.3(3) \times 10^{-9}$	0.351(1)	$6.99(8) \times 10^{6}$
775	3.10×10^{-12}	$2.38(2) \times 10^{-9}$	0.359(1)	$5.15(4) \times 10^{6}$
800	3.10×10^{-12}	$2.47(2) \times 10^{-9}$	0.361(2)	$3.84(4) \times 10^{6}$

Table 4. Fitting data for CaTa3NbO11 from 30 oC to 800 oC

T (ºC)	C_1 (Fcm^{-1})	A (Scm^{-1}rad^{-n})	n	R_1 (Ω cm)
30	$3.465(7) \times 10^{-12}$			
105	$3.445(7) \times 10^{-12}$			
198	$3.431(5) \times 10^{-12}$			
301	$3.445(7) \times 10^{-12}$			
400	$3.445(7) \times 10^{-12}$			
499	$3.462(1) \times 10^{-12}$			
599	$3.40(1) \times 10^{-12}$	$9.2(7) \times 10^{-10}$	0.383(6)	
699	3.40×10^{-12}	$6.2(1) \times 10^{-10}$	0.44(1)	$2.2(1) \times 10^{7}$
723	3.40×10^{-12}	$6.0(1) \times 10^{-10}$	0.45(1)	$1.26(3) \times 10^{7}$
750	3.40×10^{-12}	$6.0(8) \times 10^{-10}$	0.46(1)	$6.76(9) \times 10^{6}$
774	3.40×10^{-12}	$1.3(1) \times 10^{-9}$	0.413(8)	$4.09(3) \times 10^{6}$
800	3.40×10^{-12}	$1.5(1) \times 10^{-9}$	0.417(3)	$2.26(2) \times 10^{6}$

Table 5. Fitting data for CaTa2Nb2O11 from 30 oC to 800 oC

T (ºC)	C_1 (Fcm^{-1})	A (Scm^{-1}rad^{-n})	n	R_1 (Ω cm)	R_2(Ω cm)	C_2(Fcm^{-1})
30	$3.898(9) \times 10^{-12}$					
105	$3.813(6) \times 10^{-12}$					
200	$3.778(1) \times 10^{-12}$					
299	$3.745(5) \times 10^{-12}$					
398	$3.72(1) \times 10^{-12}$					
500	$3.68(1) \times 10^{-12}$	$1.6(2) \times 10^{-9}$	0.25(1)			
603	$3.68(1) \times 10^{-12}$	$3.75(5) \times 10^{-9}$	0.29(3)			
650	3.68×10^{-12}	$4.4(1) \times 10^{-9}$	0.29(2)	$1.3(1) \times 10^{7}$		
700	3.68×10^{-12}	$6.7(1) \times 10^{-9}$	0.29(1)	$3.80(7) \times 10^{6}$		
725	3.68×10^{-12}	$6.9(1) \times 10^{-9}$	0.30(1)	$1.9(4) \times 10^{6}$	$1.9(1) \times 10^{5}$	$2.2(2) \times 10^{-10}$
750	3.68×10^{-12}	$1.2(2) \times 10^{-8}$	0.28(1)	$1.07(2) \times 10^{6}$	$1.79(8) \times 10^{5}$	$1.98(9) \times 10^{-10}$
775	3.68×10^{-12}	$1.4(1) \times 10^{-7}$	0.150(8)	$7.6(2) \times 10^{5}$	$1.41(2) \times 10^{5}$	$1.47(3) \times 10^{-10}$
800	3.68×10^{-12}	$2.2(6) \times 10^{-6}$	0.044(8)	$3.49(9) \times 10^{5}$	$1.1(3) \times 10^{5}$	$1.09(4) \times 10^{-10}$